Plasma Chem Plasma Process (2017) 37:947–965
DOI 10.1007/s11090-017-9812-z

ORIGINAL PAPER

Numerical Modelling of Wood Gasification in Thermal Plasma Reactor

Ivan Hirka[1] · Oldřich Živný[1] · Milan Hrabovský[1]

Received: 16 November 2016 / Accepted: 12 March 2017 / Published online: 24 March 2017

Abstract Biomass gasification for synthesis gas production represents a promising source of energy based on plasma treatment of renewable fuel resources. Gasification/pyrolysis of crushed wood as a model substance of biomass has been experimentally carried out in the plasma-chemical reactor equipped with gas–water stabilized torch which offer advantage of low plasma mass-flow, high enthalpy and temperature making it possible to attain an optimal conversion ratio with respect to synthesis gas production in comparison with other types of plasma torches. To investigate this process of gasification in detail with possible impact on performance, a numerical model has been created using ANSYS FLUENT program package. The aim of the work presented is to create a parametric study of biomass gasification based on various diameters of wooden particles. Results for molar fractions of CO for three different particles diameters obtained by the modeling (0.55, 0.52 and 0.48) at the exit are relatively good approximation to the corresponding experimental value (0.60). The numerical results reveal that the efficiency of gasification and syngas production slightly decreases with increasing diameter of the particles. Computed temperature inhomogeneities in the volume of the reactor are strongest for the largest particle diameter and decrease with decreasing size of the particles.

Keywords Plasma modelling · CFD · Thermal plasma reactor · Biomass · Gasification · Syngas

This work has been supported by the Czech Science Foundation under Project No. GA 15-19444S.

✉ Oldřich Živný
zivny@ipp.cas.cz

[1] Institute of Plasma Physics of the CAS, v.v.i., Za Slovankou 1782/3, 182 00 Prague 8, Czech Republic

Introduction

Over the last two decades, there is a growing interest to develop sustainable alternatives to fossil resources of fuels based mainly on hydrocarbons beyond the limitations of many current biofuel production technologies, by means of resource potential, economic viability, environmental performance and safety [1]. Gasification/pyrolysis of biomass feedstock could serve as a new sustainable source of hydrogen and also synthesis gas (hereafter syngas) in gradual replacement of classical energy sources [1–5]. There are several different types of gasification technology that has been developed for conversion of biomass feedstocks. Among those technologies water thermal plasma pyrolysis/gasification offers unique features as the extremely high reaction temperature and ultra-fast reaction rate as compared to the traditional techniques [3, 4, 6].

A hybrid gas–water stabilized DC-plasma torch developed at IPP in Prague enables advantages of high input power (<160 kW) close to industrial conditions of biomass processing, high mean temperature ($\geq$ 15,000 K) and high mean enthalpy (100–270 MJ/kg) [7] making it possible to supply controlled amount of water into reaction volume already in the form of plasma, which reduces energy consumption, enhances conversion ratio and suppresses unwanted by-products. The energy demand is also lowered owing to lower plasma flow torch whereas working medium reaches higher temperatures and higher velocities enabling better controlling of the gasification process. This plasma torch has been successfully tested many times for plasma gasification of various kinds of biomass and organic materials in plasma-chemical reactor producing high quality syngas [3–5].

Models of physical and chemical processes of biomass gasification/pyrolysis including kinetics and computational fluid dynamics (hereafter CFD) have been of extensively studied over recent years [8–14]. However, majority of the published models has been focused to describe fluidized beds systems whilst substantially less computational effort has been paid to model those processes in thermal plasma reactor with special emphasis to steam plasma mixing with CO_2 and gasification of biomass particles to produce syngas as provided by experimental facility used in [3–5]. The review of the CFD computational approaches and numerical results for different types of thermal plasma reactors was reported in [15]. Nevertheless, the only CFD model of gasification processes of biomass in plasma-chemical reactor using thermal plasma as generated by water stabilized DC-plasma torch at IPP (see e.g. [3] and references ibid) published up to now is represented by a simplified model which has been recently developed by Janssens in [16] where a numerical study using ANSYS FLUENT code was carried out for several different geometries of the reactor excluding all chemical reactions of syngas production. In that model plasma and syngas were modeled as mixtures of H_2O-Ar and H_2-CO of fixed composition.

The aim of the modelling presented in the paper is to create a parametric CFD study of biomass gasification based on various diameters of wooden particles as a model substance of biomass including model of chemical reactions.

For numerical computations ANSYS FLUENT suite of programs, version 14.5 [17] has been selected.

Effects of turbulence were incorporated via both standard k-ε model and a separate implementation of turbulence and its effects on rates used chemical reactions (see "Model of Chemistry" Section). Since in study [18] it was verified that several turbulence models available in ANSYS FLUENT code provide nearly the same results in our class of problems standard k-ε model was used as the best turbulence model for all simulations

presented in this paper. The inclusion of a model describing effects of turbulence was however shown in [18] to be necessary.

The experimental measurements of the composition of syngas and other chemical species at the exit tube of the reactor were carried out several times with results published in [3].

Experimental Setup

The experimental setup of the plasma-chemical reactor and all ancillary devices is given in Fig. 1. The biomass is prepared and stored in raw material bin, from where it is transported by screw feeder directly into a reactor chamber. Black dots in Fig. 1 in the reactor chamber represents biomass falling freely downwards to the bottom of the reactor. Plasma torch is attached to the top of the reactor producing plasma flow used for heating, mixing, depolymerization, gasification and ionization of biomass making the environment in the reactor chemically highly reactive.

Processed biomass encounters plasma flow approximately 0.3 m below of the plasma entrance. The mixture of hot gases produced is cooled down in water cooling chamber that is attached to the exhaust pipe of the reactor prior to further gas analysis. The mass flow rate of cooling water is automatically controlled to maintain the temperature of exhausted gas mixture at 300 °C. In order to be able to exhaust final gas mixture into environment it is necessary to burn the final mixture because it contains dangerous or poisonous chemical species (such as carbon monoxide). This is done in combustion burner. Further details of the gasification process is given in [3–5].

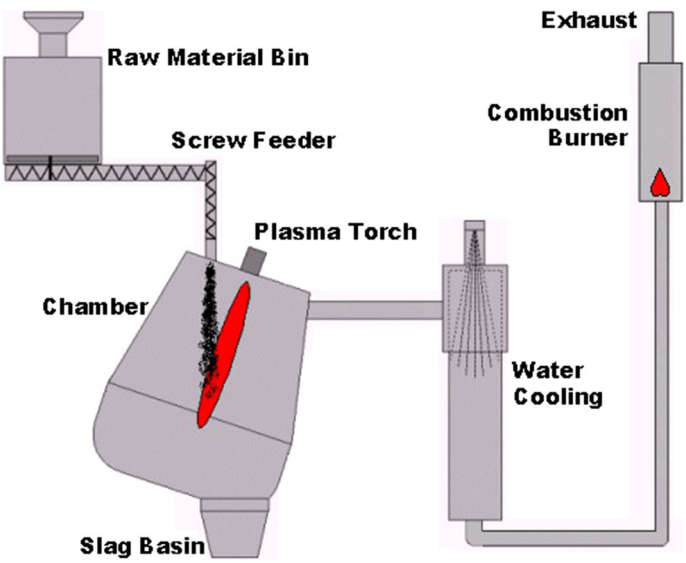

Fig. 1 Experimental setup of plasma-chemical reactor and auxiliary devices

Plasma Reactor

The internal volume of the reactor chamber is 0.206 m^3. The reactor is constructed to operate at inner wall side temperature of 1373–1673 K. Outer side of reactor walls is cooled down by slow flow of cold water. According to caloric measurements of the water used for cooling the reactor it was determined that heat losses to the walls equal 22 kW including pipes apart from this additional losses to the anode amount ca 8 kW. For detailed scheme of the reactor see Fig. 2 in "Computational Procedure" Section.

Top of the reactor has narrower (worse) insulation and so thermal losses to the top of reactor are higher than they are to other reactor walls as it follows from experiment and also from numerical simulations. There are three places in the upper part of the reactor (not visible in Fig. 2) that enable additional gases to enter the reactor. Input of such gases helps to control the composition of gas mixture in the reactor. The location of exhaust reactor tube is again in the upper part of the reactor. Such location was selected in order to force produced gases to pass through the high temperature zone that is close to or directly at the plasma jet what additionally reduces an amount of unwanted chemical species (like dioxins) present in final gas. Certain part of the biomass is gasified within its falling from waste input tube due to plasma jet. The rest (yet non-gasified part) reaches the bottom of the reactor where it is subsequently gasified due to the presence of hot gas flow.

During the process of gasification the slug basin is separated from the reactor chamber in order to keep biomass in the reactor. The amount and behaviour of non-gasified part will be discussed later (see "Results and Discussion" Section) in detail. Setup of the gasification process and also of the reactor geometry (especially the top of the reactor) is a subject to changes according to up to date level of knowledge.

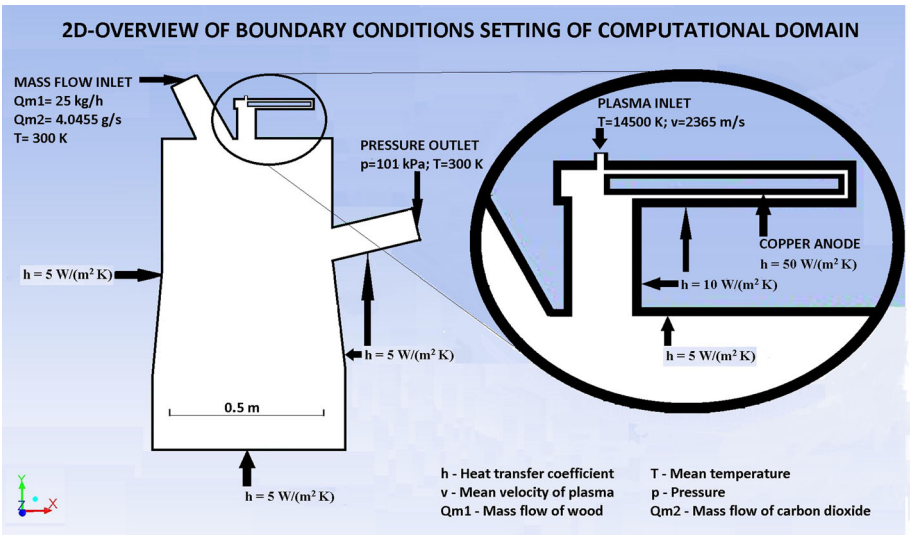

Fig. 2 2D scheme of the reactor and boundary conditions setting of computational domain

Computational Details

The Outline of the Process of Gasification

The basic framework of gasification process considered in the numerical modelling consists of several stages:

1. Solid wood in the form of idealized spherical particles of various diameters of given distribution is injected in to the reactor.
2. The solid particles enter the region heated up by plasma jet and because of high plasma temperature a heat transfer from plasma towards wooden particle is established. The heat transfer causes the wooden particles are consequently heated up and those undergo boiling and evaporating processes forming gaseous 'wood volatiles' if the temperature is sufficient. These processes are governed by temperature at the particle surface. The vaporization starts at somewhat lower temperature than boiling point, therefore these processes are simultaneous. The solid particles do not enter into chemical reaction with surrounded fluid phase species.
3. The heat transfer gradually volatilizes (or boils if boiling temperature is reached as apparent from Table 1) solid particles, resulting in a creation of a thin gas layer of 'wood volatiles' species around such the particle which contributes to volume growth of the gas phase. This process of volatilization include depolymerization and other possible chemical reactions giving rise gaseous 'monomer' of definite formula. It is assumed that each particle has a capacity of complete volatilization without unburnt fraction (char or ash), in that case volatile component fraction is one.
4. The wood volatiles arisen enter into chemical reactions forming syngas. The reaction kinetics model discern two limiting cases, namely laminar finite rate model where reaction rates are given by usual Arrhenius expressions and turbulent model where reaction rates are controlled by the turbulence.

Wooden particles represent a significant source of gas phase since during volatilization and boiling of each particle the cold solid wood is being transformed into hot gas what brings volume change of the order of 10^3. The layer of gaseous wood volatiles causes thermal insulation of wooden particle what is undesired but inevitable as wood volatiles has low thermal conductivity, which is the reason why solid particles can pass through high temperature regions of the reactor without complete volatilization.

The ability of solid particle to withstand plasma flow strongly depends on the diameter of the particle. The aim of the study presented is to determine this dependence.

Table 1 Basic physical properties of solid wood used in the model. See text for details

Physical quantity	Adopted value
Density	700 kg m^{-3}
Specific heat	2.310 kJ $kg^{-1}K^{-1}$
Thermal conductivity	0.173 W $m^{-1}K^{-1}$
Latent heat	0.0 J kg^{-1}
Vaporization temperature	513 K
Boiling temperature	650 K
Heat of pyrolysis	−4.170 J kg^{-1}
Volatile component fraction	1

Physical Properties and Input Parameters of the Model

Values of physical properties of wood and wood volatiles used in the modelling have been taken, whenever possible, from the experiment. Thus, the density of solid wood, chemical formula and corresponding molar mass of the wood volatiles have been determined experimentally at the author's workplace. The remaining properties and has been taken over from literature [19–21] or adopted from ANSYS FLUENT database [17]. The properties of solid wood used in the numerical model are summarized in Table 1.

Values of the physical properties of the wood volatiles are gathered in Table 2. The density of wood volatiles has been estimated on the basis of molar mass from ideal gas state equation.

Wooden particles enter the reactor through waste input as it is shown in Fig. 2 with the initial velocity magnitude 0.03 m s^{-1}. Total mass flow rate of wooden particles as given in Table 3 is constant and corresponds to flow rate of 25 kg h^{-1} of wood with 7% of moisture content what is one of a typical experimental value. In order to simplify the computation within reasonable limitations the moisture content of wood was set to 0 which corresponds to 23.5 kg h^{-1} of dry wood. Such decrement of wood moisture (oxidizing agent) led to required higher mass flow rate of CO_2 that enters the reactor via the same waste input as solid wood does. The input mass flow rate of CO_2 was set to 134.85 slm (4.0455 g/s) which corresponds to the stoichiometric amount (see next "Model of Chemistry" Section).

Parametric study of gasification of wood was carried out with respect to 3 different diameters of wooden particles with values given in Table 3. Diameters of particles were distributed around mean diameter within their corresponding minimum or maximum diameter value. Diameters of particles were chosen in order to represent most common conditions of gasification in the reactor. Wooden particles of mean diameter of 0.2 mm represent wood dust, particles with mean diameter 2 mm represent sawdust and particles with mean diameter 20 mm represent a size of larger pellets. Within each of the three cases of the study the particle diameters follow Rosin-Rammler diameter distribution (see [22], chap. 24), which is given by

$$y_d = \mathrm{e}^{-(d/\overline{d})^n} \qquad d_{\min} \le d \le d_{\max}, \tag{1}$$

where y_d is the mass fraction of particles with diameter greater than d, $\overline{d}$ is the mean value of d, n is the size distribution (spread) parameter, and $d_{\min}$, or $d_{\max}$ represent minimum, or maximum of d.

Physical properties of the fluid phase, namely, density (ρ), heat capacity at constant pressure (c_p), thermal conductivity (κ), and viscosity (μ), at given temperature and pressure are determined by the species dispersed. The mixture contained in the fluid phase was assumed to consist of the four individual substances, i.e. nitrogen, hydrogen, carbon

Table 2 Basic physical properties of solid wood volatiles in the model. See text for details

Physical quantity	Adopted value
Density	1.5 kg m^{-3}
Specific heat	1.5 kJ $kg^{-1}K^{-1}$
Thermal conductivity	0.0454 W $m^{-1}K^{-1}$
Viscosity	1.72 $\times 10^{-5}$ kg $m^{-1}s^{-1}$
Molar mass	38.65 g mol^{-1}

Table 3 Parameters of solid wood particles input used in the model. See text for details

Physical quantity	Adopted value
Temperature	301 K
Velocity magnitude	0.03 m s^{-1}
Total flow rate	6.46×10^{-3} kg s^{-1} (=23.5 kg h^{-1})
Min. diameter d_{min}	0.1 mm; 1 mm; 10 mm
Max. diameter d_{max}	0.3 mm; 3 mm; 30 mm
Mean diameter $\overline{d}$	0.2 mm; 2 mm; 20 mm
Spread parameter n	3.5
Number of diameters	10

dioxide, and carbon monoxide (together with possible decomposition products), and the steam plasma considered as a mixture of water and argon consisting of 95% water and 5% of argon.

To maintain the computational protocol of the model feasible the simplification assuming that the physical properties of the mixture under consideration are given by the mixing law (2) was adopted. The composition, density and thermodynamic functions including heat capacity of the systems formed by hydrogen, nitrogen, carbon monoxide, and steam plasma along with corresponding decomposition products as functions of temperature at given pressure has been computed previously at local thermodynamic equilibrium (hereafter LTE) conditions by constrained minimization of the Gibbs energy [23]. The transport properties, i.e. thermal conductivity and viscosity were calculated by Chapman–Enskog method of the solution of Boltzmann equation. These methods are described in [19]. The density of carbon dioxide in the temperature range from 300 to 2000 K has been determined by ideal gas state equation assuming the fraction above 2000 K is low.

The mixing law for a physical property z per unit of mass of the mixture of N species α means that it holds

$$z = \sum_{\alpha=1}^{N} y_\alpha z_\alpha, \tag{2}$$

where y_α is the mass fraction of the species α in the mixture. This form of mixing law was used for c_p, κ, and μ. For density ρ, the volume-weighted mixing law, however, was used which can be expressed as follows

$$\rho = \left(\sum_{\alpha=1}^{N} \frac{y_\alpha}{\rho_\alpha} \right)^{-1}.$$

The temperature dependences of the physical properties for a temperature T, 300 K $\leq T \leq$ 20,000 K, were approximated by linear piece-wise functions. The pressure dependence was omitted as the incompressible flow model was applied.

Plasma jet characteristics at the input of the reactor corresponding to the experimental conditions as reported in [4, 5] are summarized in Table 4 and used in the numerical computations.

Table 4 Plasma jet characteristics at the input of the reactor. See text for details

Physical quantity	Adopted value
Mean velocity	2635 m s^{-1}
Centerline velocity	4407 m s^{-1}
Mean temperature	14,500 K
Centerline temperature	23,000 K
Mean enthalpy	185 MJ kg^{-1}
Mean density	3.64 $\times 10^{-3}$ kg m^{-3}
Centerline density	1.23 $\times 10^{-3}$ kg m^{-3}
Reynolds number	786
Mach number	0.445
Power input	106.8 kW
Arc current	400 A
Mass flow rate	0.272 g s^{-1}

Model of Chemistry

All chemical reactions considered in the model of syngas production proceed in fluid phase, no heterogeneous reaction occurs.

As the value of latent heat of wood is not available, the heat of pyrolysis Δh° defined in Eq. (3) has been used to gather volatilization processes into one quantity, setting the value of latent heat to zero. The value of Δh° has been estimated on the basis of the experimental value ΔH reported in the first row of Table 1 of reference [20].

The process of wood volatilization

$$\text{wood}_{(s)} \rightarrow C_{1.69}H_{2.37}O_{(g)}, \quad \Delta h^{\circ} = -4.170 \text{ kJ/kg}, \tag{3}$$

where, as the negative value of specific heat of volatilization Δh° indicates, is slightly exothermic. The empirical formula $C_{1.69}H_{2.37}O$ represents one 'monomer' of gasified wood produced in our experiments in plasma reactor as determined experimentally by elemental analysis.

The adopted overall reaction scheme of syngas production from volatilized wood consists of two simultaneous irreversible reactions

$$C_{1.69}H_{2.37}O + 0.69\,CO_2 \rightarrow 2.38\,CO + 1.185\,H_2, \tag{4}$$

$$C_{1.69}H_{2.37}O + 0.121\,H_{2O} + 0.569\,CO_2 \rightarrow 2.259\,CO + 1.306\,H_2. \tag{5}$$

Reaction rates in the laminar flow follows from the chemical kinetics equations as follows

$$R_1 = k_R[C_{1.69}H_{2.37}O]^{0.2}[CO_2]^{1.3}, \tag{6}$$

$$R_2 = k_R[C_{1.69}H_{2.37}O]^{0.2}[CO_2]^{1.3}[H_{2O}]^{1.3}, \tag{7}$$

$$k_R = 1.3 \times 10^{10} e^{-1.505\times 10^8/RT}. \tag{8}$$

Chemical formulae enclosed within braces stand for molar concentration of the corresponding chemical substance. Rate exponents used in both reactions were taken over from

the database [17]. The values of activation energy and preexponential factor in Arrhenius expression (8) for the rate constant k_R were adopted from work [21].

The net source R_α of chemical species α entering into chemical reaction (4) and/or (5) then read

$$R_\alpha = \begin{cases} -M_\alpha(\nu_{\alpha,1}R_1 + \nu_{\alpha,2}R_2) & \text{for educts,} \\ M_\alpha(\nu_{\alpha,1}R_1 + \nu_{\alpha,2}R_2) & \text{for products,} \end{cases} \tag{9}$$

where $\nu_{\alpha,1}$ and $\nu_{\alpha,2}$ denotes the stoichiometric coefficient of species α entering Eqs. (4) and (5) respectively, M_α denotes the molar mass of the species α, and educts and products refer to the respective species of Eqs. (4) and (5).

If the overall rate of chemical reacting flow is driven by turbulent mixing the eddy-dissipation model is adopted for the turbulence-chemistry interaction model of Magnussen and Hjertager [24] as implemented in ANSYS FLUENT. The limiting value of net rate production R_α of species α by reaction r is given as the smaller value of the two following expressions:

$$R_{\alpha,r} = \nu_{\alpha,r}M_\alpha A\rho\frac{\varepsilon}{k}\min\frac{y_\phi}{\nu_{\phi,r}M_\phi}, \quad A = 4.0 \quad r = 1,2, \tag{10}$$

$$R_{\alpha,r} = \nu_{\alpha,r}M_\alpha AB\rho\frac{\varepsilon}{k}\frac{\sum_\chi y_\chi}{\nu_{\chi,r}M_\chi}, \quad B = 0.5 \quad r = 1,2. \tag{11}$$

Here $r = 1, 2$ stands for the reaction (4), (5), y_ϕ is the mass fraction of the particular educt ϕ, y_χ is the mass fraction of any product χ. A, B are the empirical constants and ratio ε/k is the large eddy timescale in which ε denotes turbulent dissipation rate and k turbulent kinetic energy per unit mass.

The criterion whether the flow is laminar or turbulent for the purpose of the choice of appropriate chemical reaction model depends on the fraction ε/k. If $\varepsilon/k > 1$, then the flow is considered to be turbulent, otherwise it is laminar (see [25] and reference therein for more details). The values of k and ε are computed in terms of standard k-ε turbulence model as implemented in ANSYS FLUENT (see next section).

Governing Equations

For more detailed description of theory underlying the numerical model used see [25] and reference therein.

Mass conservation, or continuity equation is expressed as

$$\frac{\partial\rho}{\partial t} + \nabla\cdot(\rho\mathbf{v}) = S_\mathrm{m}, \tag{12}$$

where ρ is the local density, $\mathbf{v}$ is the fluid velocity, and the source term S_m express mass added to the fluid phase from the dispersed second phase.

Conservation of momentum in an inertial reference frame is given as

$$\frac{\partial\rho\mathbf{v}}{\partial t} + \nabla\cdot(\rho\mathbf{v}\mathbf{v}) = -\nabla p + \nabla\cdot\overline{\tau} + \rho\mathbf{g} + \mathbf{F}, \tag{13}$$

where p is the static pressure, $\overline{\tau}$ is the stress tensor [see below Eq. (14)], and $\mathbf{g}$, and $\mathbf{F}$ stand for the gravitational force and external body forces respectively. Stress tensor $\overline{\tau}$ is defined as follows

$$\overline{\tau} = \mu\left[\left(\nabla\mathbf{v} + \nabla\mathbf{v}^T\right) - \frac{2}{3}\nabla\cdot\mathbf{v}\mathsf{I}\right], \tag{14}$$

where μ is the molecular viscosity, $\mathbf{v}$ is the fluid velocity and I is the unit tensor.

Conservation of energy in terms of energy equation is

$$\frac{\partial\rho E}{\partial t} + \nabla\cdot[\mathbf{v}(\rho\mathbf{E} + \mathbf{p})] = \nabla\cdot\left(\kappa_{\text{eff}}\nabla T - \sum_{\alpha=1}^{N} h_\alpha\mathbf{J}_\alpha + \overline{\tau}\cdot\mathbf{v},\right) + S_\text{h}, \tag{15}$$

where the right-hand side include energy transfer due to conduction, species diffusion, viscous dissipation, and as S_h, heat of chemical reactions or other defined sources, respectively. κ_{eff} is the effective heat conductivity, $\kappa_{\text{eff}} = \kappa + \kappa_\text{t}$, while κ_t is turbulent thermal conductivity defined according to standard k-ε model. For the energy E per unit mass of (15) it holds

$$E = h - \frac{p}{\rho} + \frac{v^2}{2}, \tag{16}$$

where total specific enthalpy h of the fluid considered in an ideal gas state can be expressed as

$$h(T) = \sum_{\alpha=1}^{N}[y_\alpha\,\Delta h_\alpha^\circ(T) + \Delta_\text{f}\,h_\alpha^\circ(T_\text{ref})], \tag{17}$$

$$\Delta h_\alpha^\circ(T) = \int_{T_\text{ref}}^{T} c_{p_\alpha}^\circ(T)\,\text{d}T, \tag{18}$$

and where Δh_α° denotes standard specific enthalpy of the species α, relative to reference temperature T_ref (T_ref = 298.15 K for the pressure based solver), $\Delta_\text{f}\,h_\alpha^\circ$ is standard specific enthalpy of formation, and $c_{p_\alpha}^\circ$ is standard specific heat capacity of the species α at constant pressure.

Species transport follows from species conservation equations, in which mass fraction y_α of the species α, $\alpha = 1, 2, \ldots, N$, in fluid phase satisfy convection-diffusion equation

$$\frac{\partial(\rho y_\alpha)}{\partial t} + \nabla\cdot(\rho\mathbf{v}y_\alpha) = -\nabla\cdot\mathbf{J}_\alpha + R_\alpha, \quad \alpha = 1, 2, \ldots, N-1 \tag{19}$$

where R_α is the net rate of production of species α by chemical reaction as defined by (9), and where diffusion flux $\mathbf{J}_\alpha$ flows is given as

$$\mathbf{J}_\alpha = -D_\text{T}\alpha\frac{\nabla T}{T} - \begin{cases}\rho D_{\text{m}\alpha}\nabla y_\alpha & \text{for laminar flows;}\\ \rho(D_{\text{m}\alpha} + D_{\text{t}\alpha})\nabla y_\alpha & \text{for turbulent flows.}\end{cases} \tag{20}$$

Here $D_{\text{m}\alpha}$ is the mass diffusion coefficient for species α in the mixture, $D_\text{T}\alpha$ is the thermal (Soret) diffusion coefficient, and $D_{\text{t}\alpha}$ is the turbulent diffusivity defined as follows

$$D_{\text{t}\alpha} = \frac{\mu_\text{t}}{\rho\text{Sc}_\text{t}}, \tag{21}$$

in which μ_t is the turbulent viscosity and Sc_t is the turbulent Schmidt number (default is 0.7).

Trajectory of discrete phase particle follows from the equation

$$\frac{\mathrm{d}\mathbf{u}_\mathrm{p}}{\mathrm{d}t} = F_\mathrm{D}(\mathbf{v}-\mathbf{u}_\mathrm{p}) + \frac{\mathbf{g}(\rho-\rho_\mathrm{p})}{\rho_\mathrm{p}} + \mathbf{F}, \tag{22}$$

where $\mathbf{u}_\mathrm{p}$ denotes the particle velocity, $\mathbf{v}$ is the fluid phase velocity, $\mathbf{F}$ is the additional acceleration, and $F_\mathrm{D}(\mathbf{v}-\mathbf{u}_\mathrm{p})$ is the drag force per unit particle mass. F_D is defined by following expression

$$F_\mathrm{D} = \frac{18\mu\, C_\mathrm{D}\mathrm{Re}}{24\rho_\mathrm{p}\, d_\mathrm{p}^2}, \tag{23}$$

in which C_D is the dimensionless drag coefficient, ρ_p is the particle density and d_p is the instant particle diameter. Re is the relative Reynolds number, defined as

$$\mathrm{Re} = \frac{\rho d_\mathrm{p}|\mathbf{u}_p-\mathbf{v}|}{\mu}. \tag{24}$$

The turbulence model adopted for the computation of the turbulence kinetic energy k and its dissipation rate ε as used in Eqs. (10) and (11) is based on solution of two separate transport equations model proposed by Launder and Spalding [26].

The transport equations for the standard k-ε model are reported in [25].

Computational Procedure

As the thermal plasma reactor does not possess axial symmetry nor any other symmetry it was necessary to carry out 3 dimensional (3D) computations. The 2D scheme of the reactor with boundary conditions setting is depicted in Fig. 2

The whole computational protocol as described in previous paragraph in terms of governing equation system was carried out using ANSYS FLUENT program package. The exception is the calculation of composition of the plasma system under LTE conditions which were performed using different program (see below). For more details on the solver used in the computations, see [25].

For standard k-ε model used for description of turbulence two assumptions were applied: the plasma flow is turbulent and subsonic while while effects of molecular viscosity are negligible. Radiation effects and magnetic field were neglected and gravitational force is included in computations. Steam plasma is considered to be in LTE. No user defined sources were implemented to governing equations. Total volume of calculation domain (i.e. inner volume of the reactor chamber) is 0.206 m^3. All numerical simulations presented here were carried out corresponding to real dimensions at scale ratio 1:1. Dimensions of the domain embrace not only the reactor chamber itself but also the exhaust pipe and all parts necessary for fixing of the plasma torch to the reactor chamber. As the real flow in the reactor is only mildly compressible we decided to neglect the compressibility effects on the flow and to use incompressible approach and pressure based solver with absolute velocity formulation in all the calculations. SIMPLE scheme was used for pressure-velocity coupling. Green-Gauss cell based gradient evaluation method was used for computations of gradients of any scalar φ at the corresponding cell centre. Values of the physical properties for the incompressible fluid phase species as functions of the temperature were given in terms of linear-piecewise functions as described in "Physical Properties and Input Parameters of the Model" Section.

Grid used in all our simulations contained approximately 1.2 million nodes and is of varying node density. Grid was purely tetrahedral because in majority of reactor chamber it is not possible to determine the prevailing direction of flow. Determination of flow direction was possible only in small area representing a part of internal volume of the torch itself and hence in such area the hexahedral uniform grid was used. Third-order MUSCL scheme was applied to the grid to reduce numerical diffusion and due to the use of this scheme the computation possesses third-order accuracy for diffusive and conductive terms. All simulations were performed with single precision.

All boundary conditions of the computational domain were set according to known experimental values since major purpose of this modelling is to find out distributions of physical properties in internal parts of the reactor. Heat losses to the reactor walls were always modelled by prescribed heat flux and only in one special case the wall temperature of the reactor was constantly set to 1300 K because such wall temperature is usually obtained at the experiment. This heat flux was not constant but was computed via conduction of heat in solid reactor walls with certain width of walls and with subsequent convection of heat via cooling liquid (water) that is present at outer side of reactor walls. The temperature of this cooling liquid was prescribed and kept constant. This heat flux to the walls was determined by constant heat transfer coefficient that was the same for all parts of reactor chamber representing cumulative thermal insulation ability of all ceramic and other insulation layers. Used values of heat transfer coefficients (see Fig. 2) are as follows: 5 $Wm^{-2}K^{-1}$ for the reactor chamber and connected pipes; 10 $Wm^{-2}K^{-1}$ for purely metallic insulating parts; 50 $Wm^{-2}K^{-1}$ for copper anode. Width of reactor walls for the need of the computation of heat losses were 0.4 m for reactor chamber and 0.1 m for pipes. Width of anode wall was 5 mm. Width of walls made of purely metallic parts was 20 mm. Temperature of cooling liquid was constantly set to 300 K. All these setting was made in order to achieve thermal losses of 22 kW to the reactor walls (including pipes) and separately of 8 kW to the anode.

The discrete phase (i.e. wooden particles) in the ANSYS FLUENT code is modelled via Euler-Lagrangian discrete phase model. Discrete phase (that is dispersed into the viscous continuum) can exchange mass, momentum and energy with the continuum. The wooden particle trajectories are computed individually only every 5th iteration of the fluid phase.

In the present model the trajectory of each solid particle was determined by solution of the corresponding equations of motion including three forces, namely, drag force, gravitational force, and thermophoretic force.

The node density within the reactor chamber itself is nearly constant because physical conditions in the reactor chamber are not extremely spatially different. There are only two most visible interfaces where the density of computational grid is greatly changed: between arc area and plasma inlet pipe and between plasma inlet pipe and the reactor.

The whole computational process is iterative with average number of approximately 30,000 iterations per one computation until converged solution is reached. This number is higher than usual because some boundary conditions and also several other parameters (mainly mean diameter of wooden particles and mass flow of wooden particles) can not be set to the values used in the experiment at the beginning of the computation because of a numerical instability.

After reaching partially converged solution for intermediate values of boundary conditions and parameters it is possible again to adjust these values more towards desired boundary conditions.

Calculation of the Composition at LTE

Input parameters for the equilibrium calculation were based on the following assumptions: injected gas flow consists of 98.75CO_2 and 1.25% of N_2, and flow rate is 6.6 g/s; steam plasma flow rate is 0.271 g/s and consists of H_2O (95%) and Ar (5%); wood of summary formula $C_{1.69}H_{2.37}O$ contains additionally 7% of H_2O and its feeding rate is 6.96 g/s. These parameters correspond to amount of substances as follows: 0.4305 mol of C, 0.4786 mol of H, 0.0059 mol of N, 0.5046 mol of O, and 0.0003 mol of Ar.

The method used for the equilibrium calculations was based on non-stoichiometric algorithm [23] by means of constrained minimization of total Gibbs energy of the system fulfilling mass balance conditions at given temperature and pressure [27]. Standard thermodynamic functions required for all components considered in the heterogeneous system used for the calculations has been taken from database system [28]. The system under consideration was formed by total number of 72 species including two species in condensed phase (graphite and liquid water).

Results and Discussion

All results of the simulations presented in this section are converged. A numerical simulation in this study is considered to be converged if all scaled residuals fall below the value of 10^{-3} and scaled residual for energy below the value of 10^{-6}. With respect to the fact that some residuals had been still little above the threshold values denoting full convergence the computations were continued and results repeatedly checked in order to verify if the solutions were constant with increasing number of iterations.

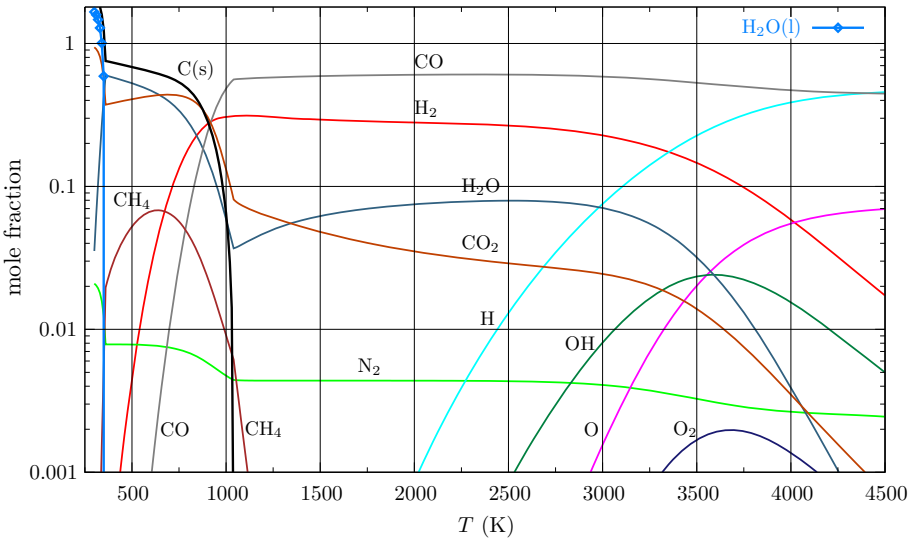

Fig. 3 Equilibrium composition of wood gasification products in temperature range from 300 to 4500 K at atmospheric pressure. Abundances of condensed phases, namely liquid water and solid carbon are expressed as amount of substance of the corresponding condensed phase per one mol of gaseous phase of the system. Argon as non-reactive species is not shown. See text for details

Considering LTE conditions, the calculated composition (Fig. 3) is in close agreement with the measured values (see [3]), however at low temperatures below ca 1000 K the calculated fractions of CO and H_2 as underestimated no longer properly correspond to the experiment.

Assumption of LTE is adequate if the processes tending towards the equilibrium are sufficiently fast which is the case of chemical reactions at atmospheric pressure and high temperatures. If the temperature is decreasing, the departures from the chemical equilibrium becomes more important because of activation barrier and the chemical composition is driven by kinetics. As apparent from Fig. 3 in low temperature region below ca 1000 K the equilibrium composition driven by thermodynamics prefers solid carbon formation to CO and with further decreasing temperature the proportion of the methane, with maximum at 700 K, predominates over syngas formation suppressing CO and H_2. The experimental composition of the output gases have corresponded to the "frozen" composition near 1300 K.

Since it is desirable to adequately determine composition also in the regions of low temperatures, the inclusion of a model chemical kinetics is indispensable.

The overall reaction scheme is expressed by the irreversible reactions (4) and (5) which allows to create a realistic model of the gasification comparable with the available experimental results, which would not be possible under LTE assumption.

The values adopted for the experimental molar fractions of the produced gases forming syngas has been critically evaluated on the basis of repeated measurements on the exit (see [3–5]) corresponding to the typical operational conditions as considered in this study.

The computed distributions of mole fractions of CO and H_2 are depicted in Fig. 4. The evaluated experimental mole fraction of CO is 0.6 which agree well with the computed results, namely 0.55, 0.52, and 0.48 obtained for three different mean particles diameters, i.e. 0.2 mm, 2 mm, and 20 mm, respectively. The experimental value of mole fraction of H_2 is 0.3 which is also in close agreement with the computed values, i.e. 0.27, 0.25, and 0.22 for the same sequence of mean particle diameters. This trend observed in decreasing of syngas components mole fraction with increasing mean particle diameter is caused by worsened mixing of reacting gases and wood volatiles with plasma flow in the case of larger particles because of longer volatilization time. In contrast with nearly homogeneous mixing for the particles of mean diameter 0.2 mm (see Fig. 4a, d), in the cases of larger diameters mixed gases form thin reaction layer in the middle of the reactor (Fig. 4b, c, e, f) whereas steam plasma and CO_2 remain in the upper region of the reactor chamber and wood volatiles occupy lower part of the reactor chamber. Even though the chemical reactions occur only in the thin layer the reaction rate is considerably higher than macroscopic flow low which still results to the high reaction yield.

Temperature distributions for three mean diameters 0.2, 2 and 20 mm are shown on Fig. 5a–c. In this sequence of temperature distributions an extent of an efficiency of mixing of thermal plasma flow with cold gas flow and with flow of solid particles is presented. As apparent from Fig. 5 the temperature is not uniformly distributed in whole volume of the reactor chamber in which the upper part is of higher temperature than the lower one. The high temperature area located in upper right corner of the reactor chamber slightly increases with increasing the particle diameter and within the reactor is suited for decomposition of possible unwanted reaction by-products. This inhomogeneity is caused by insufficient energy drain of cold gas and cold solid particles injected through waste input. The level of temperature homogeneity is highest for the smallest particle diameter (Fig. 5a) and it subsequently decreases with increasing diameter of gasified particles. This tendency can be attributed to the larger effective surface of the smallest particles in respect

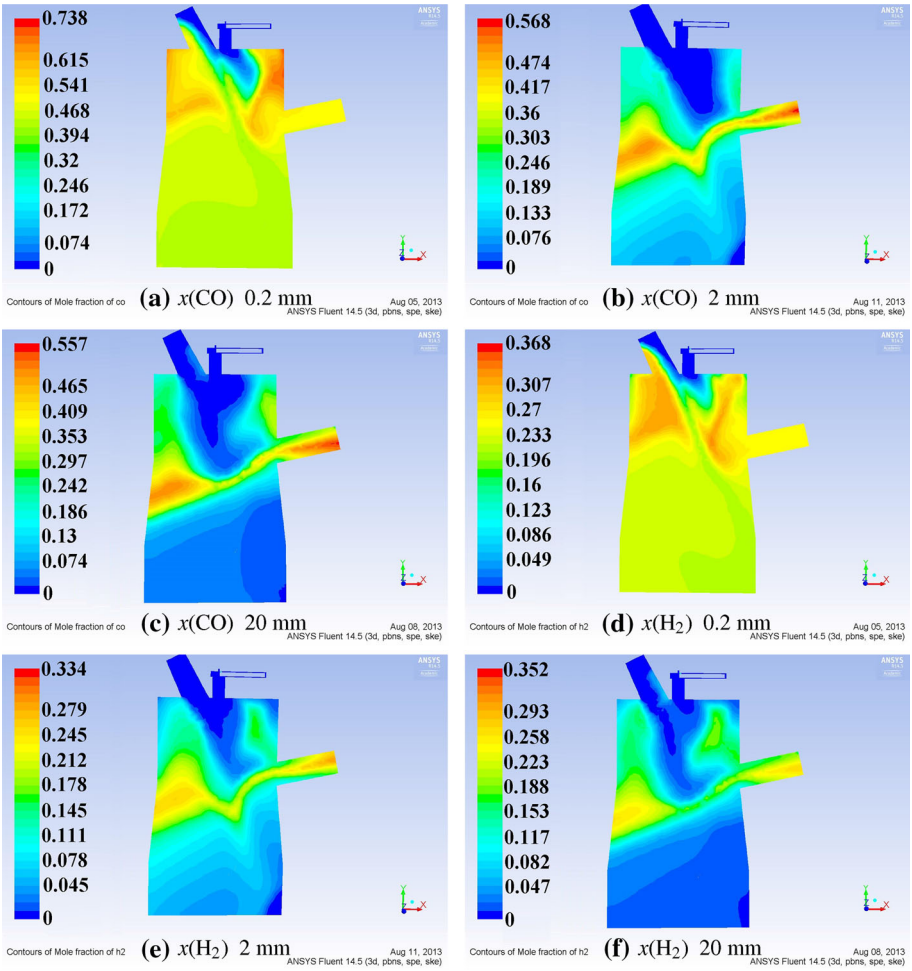

Fig. 4 2D slice of mole fraction distribution of CO and H_2 for three different diameters of wood particles, 0.2, 2, and 20 mm

to the interaction with surrounding plasma flow and reacting gas. As a consequence, the smallest particles are capable of mixing hot and cold flows as they withdraw energy from the upper part of the reactor and carry it towards the bottom area. This effect of temperature homogenization is the most visible in Fig. 5d–f.

Computed 3D distribution of temperature inside of the reactor chamber is shown in Fig. 6. Since the computational grid is very dense mainly distributions of temperature on inner reactor walls (representing the boundary of the computational domain) are visible. In Fig. 6c there is the largest hot area at the top of the reactor chamber of all three cases what indicates lowest flow mixing. Note also the heat energy is up to some extent exhausted by exhaust pipe out of the reactor what is indicated by orange and yellow colour at the upper parts of the exhaust tube. This exhausting of heat energy is lower in Fig. 6b and lowest in Fig. 6a.

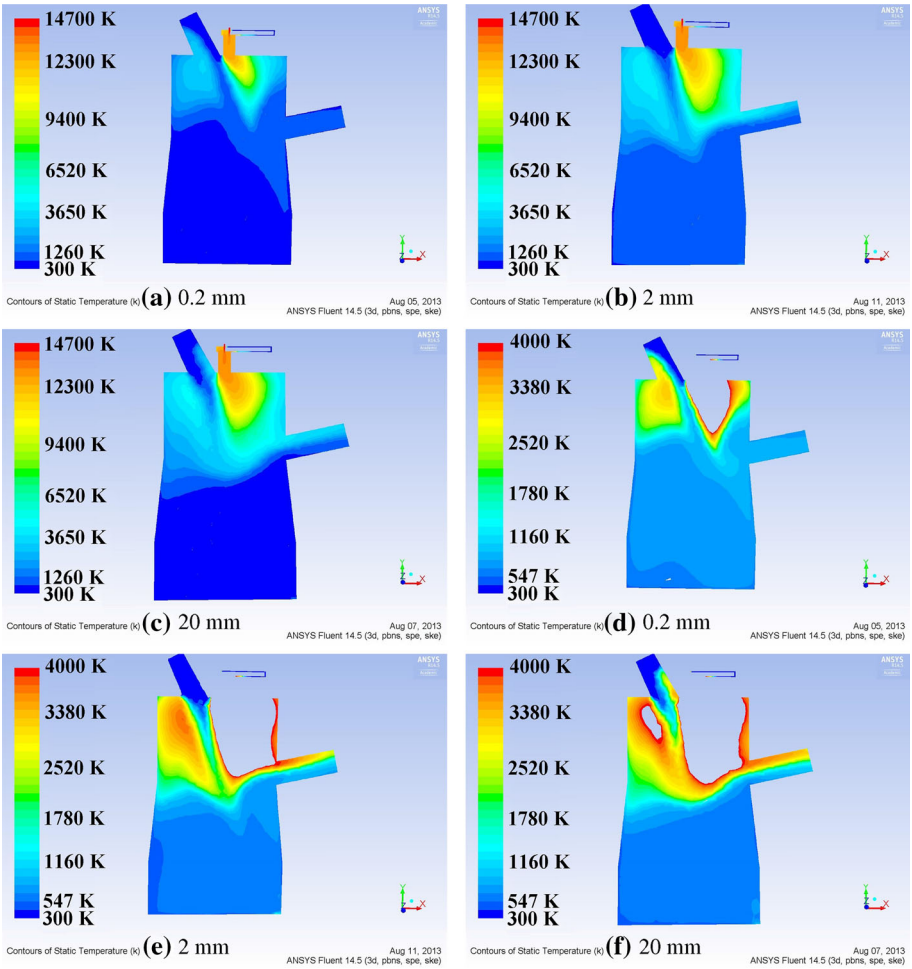

Fig. 5 2D slice of temperature distribution for three different diameters of wood particles, 0.2, 2, and 20 mm. **a–c** show temperature distribution within the range 300–14,700 K; **d–f** show temperature distribution within the range 300–4000 K

All these observations prove that mixing is better with decreasing diameter of the particles.

Importantly, the numerical results show that some wooden particles can pass through plasma jet without complete gasification and fall down to the bottom of the reactor where they are gradually gasified as well. However, such delayed gasification of wooden particles at the bottom of the reactor does not affect the reaction yield of syngas as shown in Fig. 4.

Another effect predicted by the numerical model and verified experimentally represents backflow of syngas. The backflow of syngas from reaction chamber to the anode area has been already modelled in the past on the basis of the presence syngas forming components in the vicinity of the anode [18] as well as by the direction of the corresponding velocity vector [16]. In contrast to these previous simulations in this study both velocity vector and chemical composition in the anode area has been computed. The typical value of mole

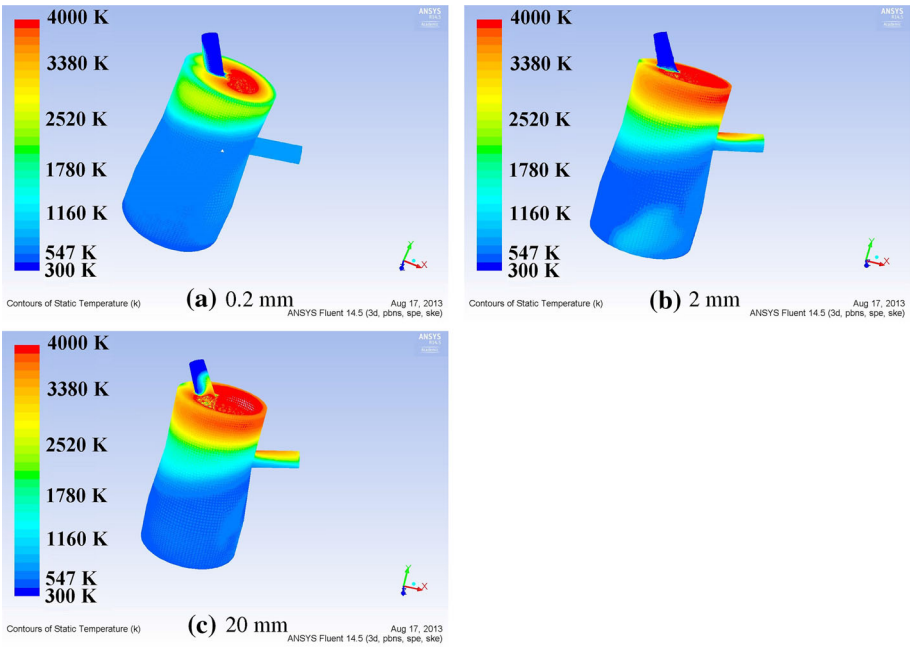

Fig. 6 3D temperature distribution for three different diameters of wood particles, 0.2, 2, and 20 mm. **a**–**c** show temperature distribution within the range 300–4000 K

fraction of CO at the top of the anode is 8.5×10^{-4} which is very small in magnitude, however, during long-term operation of the torch this leads to a char formation at the anode surface. This char formation has been experimentally observed.

The computed average speed of gas mixture in the anode area equals approximately to 0.05 ms^{-1}. This speed is higher at the top of the anode area and it increases with decreasing of distance from plasma jet that operates here also as a pump accelerating the gas. The results obtained for all three mean particle diameters has been nearly the same.

Conclusions

A parametric CFD study of biomass gasification processes in plasma-chemical reactor using an unique hybrid gas–water stabilized plasma torch has been carried out.

Gasification model, employing Euler–Lagrange approach and chemical kinetics, has been based on description of physical and chemical processes in thermal plasma flow including gas mixing, interaction of injected biomass with plasma, its volatilization and subsequent chemical reactions along with induced physical changes in the volume of reactor chamber. A model substance of biomass has been represented by spherical wooden particles distributed around three different mean diameters, namely 0.2, 2, and 20 mm. Modelling of the gasification processes has been focused to the area inside closed plasma reactor equipped by gas and water stabilized DC-plasma torch under typical operational conditions with input torch power around 100 kW and mean enthalpy of 185 MJ/kg and with feeding rate of crunched wood of 25 kg/h.

Among the computational results obtained in this study for which the experimental data are available the theoretical composition of produced syngas formed by CO and H_2, on the exit show close approximation of the experiment—the model has predicted values of mole fractions to be 0.55, 0.52, and 0.48 for mean diameter 0.2, 2, and 20 mm, respectively in the case of CO with experimental value 0.6, and 0.27, 0.25, and 0.22 in the case of H_2 with experimental value 0.3 for the same sequence of mean diameters.

As apparent from the numerical results the efficiency of gasification and syngas production slowly decreases with increasing diameter of used particles. Yield lowering of syngas for larger particles is caused both by lower total transfer of heat to larger particles, causing losses of heat energy, and by the fact that some small amount of particles are exhausted prior to complete volatilization.

The computed temperature distribution has revealed inhomogeneities in the volume of the reactor which were known before, however not experimentally accessible in the whole reactor volume. This effect caused by energy drain of cold gas and cold solid particles injected into reactor volume is most important for the largest particle diameter and decreases with decreasing size of particles.

An other important result is the verification of backflow of gases from the reactor chamber towards anode area. This backflow is observed experimentally and it causes unwanted condensation of carbon at this area.

The numerical model used in the work presented has comprised both CFD and chemical kinetics that is published, in relation to the gasification processes in the plasma-chemical reactor as used at IPP in Prague, for the first time.

References

1. Review of technologies for gasification of biomass and wastes, NNFCC project 09/008, E4Tech, June (2009)
2. Tang L, Huang H, Hao H, Zhao K (2013) Development of plasma pyrolysis/gasification systems for energy efficient and environmentally sound waste disposal. J Electrost 71:839–847
3. Hlína M, Hrabovský M, Kavka T, Konrád M (2014) Production of high quality syngas from argon/water plasma gasification of biomass and waste. Waste Manag 34:63–66
4. Hrabovský M, Konrád M, Kopecký V, Hlína M (2006) Pyrolysis of wood in arc plasma for syngas production. High Temp Mater Process 10:557–570
5. Hlína M, Hrabovský M, Kopecký V, Konrád M, Kavka T, Skoblja S (2006) Plasma gasification of wood and production of gas with low content of tar. Czechoslovak J Phys Suppl B 56:B1179–B1184
6. Kawai Y, Ikegami H, Sato N et al (eds) Industrial plasma techmology: applications from environmental to energy technologies, Chap. 6. Wiley, Weinheim (2010)
7. Hrabovský M (2002) Generation of thermal plasmas in liquid stabilized and hybrid dc-arc torches. Pure Appl Chem 74:429–433
8. di Blasi C (2008) Modeling chemical and physical processes of wood and biomass pyrolysis. Prog Energy Combust Sci 34:47–90
9. de Sousa-Santos ML (2010) Solid fuels. Combustion and gasification, vol 2. CRC Press, Boca Raton
10. Gómez-Barea A, Leckner B (2010) Modeling of biomass gasification in fluidized bed. Prog Energy Combust Sci 36:444–509
11. Ahmed TY, Ahmad MM, Yusup S, Inayat A, Khan Z (2012) Mathematical and computational approaches for design of biomass gasification for hydrogen production: a review. Renew Sustain Energy Rev 16:2304–2315
12. Singh RI, Brink A, Huppa M (2013) CFD modeling to study fluidized bed combustion and gasification. Appl Therm Eng 52:585–614
13. Xue Q, Fox RO (2014) Multifluid CFD modeling of biomass gasification in polydisperse fluidized bed gasifiers. Powder Technol 254:187–198

14. Martinéz-Lera S, Ranz JP (2016) On the development of a wood gasification modelling approach with special emphasis on primary devolatilization and tar formation and destruction phenomena. Energy 113:643–652
15. Mashayak SY (2009) CFD modeling of plasma thermal reactor for waste treatment. Thesis, Purdue University, West Lafayette, Indiana, M.Sc
16. Janssens S (2007) Modeling of heat and mass transfer in a reactor for plasma gasification using a hybrid gas-water torch. Thesis, Ghent University, Belgium, M.Sc
17. ANSYS FLUENT (2010) release 14.5
18. Hirka I, Hrabovský M (2010) Three-dimensional modelling of mixing of steam plasma jet with nitrogen in thermal plasma reactor. High Temp Mater Proc 14:1–8
19. Křenek P (2008) Thermophysical properties of H_2O-Ar plasmas at temperatures 400–50,000 K and pressure 0.1 MPa. Plasma Chem Plasma Process 28:107–122
20. Cho J, Davis JW, Huber GW (2010) The intrinsic kinetics and heats of reactions for cellulose pyrolysis and char formation. Chem Sus Chem 3:1162–1165
21. Miller RS, Bellan J (1997) A generalized biomass pyrolysis model based on superimposed cellulose, hemicellulose and lignin kinetics. Combust Sci Technol 126:97–128
22. ANSYS FLUENT (2010) release 14.5 User's Guide
23. Smith WR, Missen RW (1982) Chemical reaction equilibrium analysis. Wiley, New York
24. BF Magnussen, BH Hjertager (1976) On mathematical models of turbulent combustion with special emphasis on soot formation and combustion In: 16^{th} Symposium (International) on Combustion. The Combustion Institute , pp. 719–729
25. ANSYS FLUENT (2010) release 14.5, Theory Guide, ANSYS Inc
26. Launder BE, Spalding DB (1972) Lectures in mathematical models of turbulence. Academic Press, London
27. Coufal O, Živný O (2011) Composition and thermodynamic properties of thermal plasma with condensed phases. Eur Phys J D 61:131–151
28. Coufal O, Sezemský P, Živný O (2005) Database system of thermodynamic properties of individual substances at high temperatures. J Phys D Appl Phys 38:1265–1274